Ionics (2020) 26:2633–2641
https://doi.org/10.1007/s11581-019-03377-8

ORIGINAL PAPER

Sensitive detection of estriol with an electrochemical sensor based on core-shell N-MWCNT/GONR-imprinted electrode

Xiaodong Xin[1] · Shaohua Sun[1] · Mingquan Wang[1] · Ruibao Jia[1]

Received: 8 October 2019 / Revised: 20 November 2019 / Accepted: 27 November 2019 / Published online: 12 December 2019

Abstract

A highly sensitive and selective electrochemical sensor based on a new molecularly imprinted polymer was proposed for the detection of estriol. Nitrogen-doped multi-walled carbon nanotube/graphene oxide nanoribbons (N-MWCNT/GONRs) were synthesized by the facile partially unzipping of N-MWCNTs with the help of microwave irradiation. The molecularly imprinted electrochemical sensor was fabricated by electrochemically polymerization of pyrrole onto N-MWCNT/GONR-modified Au electrode. Under the optimum condition, the sensor showed good response in the range of low concentrations from 0.1 $\mu g \cdot mL^{-1}$ to 20 $\mu g \cdot mL^{-1}$ with the detection limit (3σ, RSD $\leq 5\%$) of 2 $ng \cdot mL^{-1}$. Estradiol, diethylstilbestrol, oestrone bisphenol A, and ethinyloestradiol had negligible interference in the determination of estriol even when the concentration molar ratio reaches 50:1. The developed sensor had been applied to the reliable analysis of estriol in clinic samples and in real water samples with satisfactory results.

Keywords Molecular imprinted sensor · N-MWCNT/GONRs · Estriol · Pyrrole · Electropolymerization

Introduction

Estriol (E3) is one of the major urinary metabolites of ovarian estradiol, produced throughout a woman's reproductive years and increases to high levels during pregnancy. E3 plays an important role in the monitoring of fetal well-being and development during pregnancy. It has also been found to be associated with breast cancer [1]. Pharmaceutical estriol compounds are believed to be harmful to animals and the environment since they have high biological activity and are not readily degraded [2]. Accurate determination of E3 concentrations in the human serum, plasma, or urine, during pregnancy, helps to judge the content and the development of the fetus.

E3 levels in urine, serum, and amniotic fluid is often measured by high-performance liquid chromatography using various detectors [3, 4], gas chromatography-mass spectrometry [5], micellar electrokinetic chromatography [6], and enzyme immunoassay [7]. Especially, electrochemical sensor is preferred because of its reliability, fast response, low cost, simple operation, short analysis time, high sensitivity, good selectivity, the potential for miniaturization, and the possibility of in situ analysis. At the present time, there are only a few publications reporting the electrochemical determination or behavior of estriol [8–10].

To increase the sensitivity and selectivity of electrochemical sensor, various nanomaterials have been used [11–14]. Carbon nanotubes (CNTs) were widely utilized in electrochemical analysis [15, 16]. Recently, graphene-based nanomaterials have gained much more attention for electrochemistry applications, including energy storage and sensing [17–19].

In order to enhance the sensitivity of the sensor, graphene oxide nanoribbons (GONRs) fabricated by the microwave-assisted facile unzipping of multi-walled carbon nanotubes (MWCNTs) were introduced owing to their unique properties involving large surface area, excellent conductivity, subtle catalytic ability, and adsorption ability. GONRs have high

Electronic supplementary material The online version of this article (https://doi.org/10.1007/s11581-019-03377-8) contains supplementary material, which is available to authorized users.

✉ Ruibao Jia
jiaruibao1968@163.com

[1] Shandong Province Water Supply and Drainage Monitoring Center, Jinan 250000, China

density of unoccupied electronic states and enriched oxygen-based functionality at the edge of the graphene-like structures showed excellent electrochemical performance [20]. Moreover, N-doped nanomaterials have been employed in many fields including supercapacitors, electrocatalysis, and electrochemical biosensors owing to the high electric conductivity and large amount of edge sites [21–25]. The electrocatalytic activity of N-doped carbon materials has been extensively studied [26–28]. The electrocatalytic properties of N-doped nanocarbons depend strongly on the bonding configuration of N atoms on the surface of carbon nanomaterials.

Molecularly imprinted technique (MIT) has been demonstrated as a desirable technique in analytical field [29–31]. Molecularly imprinted polymer (MIPs) can act as artificial antibodies toward the target molecules for analytical purposes due to the complementarity in functional group orientation and spatial structure [32, 33]. Poly(pyrrole) is one of the most extensively studied conducting polymers and is considered as the most promising material for the development of sensor devices because of its unique properties such as, high conductivity, facile preparation, efficient polymerization, stability in ambient conditions, and thickness controllability. Composite materials based on the coupling of poly(pyrrole) and graphene materials with the aim of combining the properties of these materials, have been intensively studied in some publications [34–36]. These composite materials have shown to possess complementary properties of the individual components with a synergistic effect [37]. The desirable merging of properties of poly(pyrrole) and graphene leads to a superior performance of the resulting sensing materials.

In this study, a novel molecularly imprinted electrochemical sensor was fabricated by electrochemical polymerization of pyrrole onto nitrogen-doped multi-walled carbon nanotube/graphene oxide nanoribbon (N-MWCNT/GONR)-modified Au electrode for sensitive detection of estriol. In some studies, pyrrolic-N functionalities have been reported as catalytically active groups [38, 39]. N-MWCNT/GONRs were synthesized from the facile partially unzipping of N-MWCNTs with the help of microwave irradiation. Parameters controlling the performance of the molecularly imprinted sensor were investigated and optimized. This fabricated electrochemical sensor was used for determination of estriol in clinical samples and in real water samples with satisfactory results.

Materials and methods

Apparatus and reagents

Nitrogen-doped multi-walled carbon nanotubes (N-MWCNTs) were used as received from Mitsui & Co. (product name, NCT tube; diameter = 40~60 nm; length ≥ 10 μm). Sulfuric acid (H_2SO_4), phosphoric acid (H_3PO_4), and potassium permanganate ($KMnO_4$) were purchased from J.T. Baker. Estriol was obtained from Sigma. All solutions were prepared with deionized water with a resistivity of 18 MΩ/cm.

Transmission electron microscope (TEM) images were obtained from H-800 microscope (Hitachi, Japan). X-ray photoelectron spectroscopy (XPS) measurements were recorded on an XSA-800 (Kragos Co., England) with Al Kα X-ray radiation as the X-ray source for excitation. Fourier transform infrared spectroscopy (FTIR) spectra of the samples were recorded at room temperature in the spectral range of 4000–400 cm^{-1} using the Perkin-Elmer Spectrum One FTIR spectrometer (Perkin–Elmer, United States). Raman spectroscopy was analyzed at a laser wavelength of 633 nm by a Raman Spectrometer NEXUS 670 (Thermo Nicolet, United States). Brunauer–Emmett–Teller (BET) analysis of C-MWCNs was performed on a Micromeritics ASAP 2020 surface area and porosity analyzer (Quantachrome, USA). All electrochemical measurements were performed on a CHI760E electrochemical workstation (Chenhua Instrument Shanghai Co., Ltd., China). A conventional three-electrode system was used for all electrochemical measurements: a gold electrode (GE, 3 mm in diameter) as working electrode, a platinum wire electrode as the counter electrode, and a saturated calomel electrode (SCE) as the reference electrode.

Synthesis of N-MWCNT/GONRs

According to Sun's report [20], N-MWCNTs (0.05 g) were suspended in 9:1 H_2SO_4/H_3PO_4 and treated with a microwave reactor with the power set 140 °C for 2 min. After the addition of $KMnO_4$ (0.25 g) to the solutions, the solutions were treated with the same microwave power at 65 °C for 4 min. The solutions were filtered through a Millipore membrane (0.1 μm pore size), and the solid products (N-MWCNT/GONRs) were washed with water several times.

Preparation of the E3 electrochemical sensor

MIP was constructed by electropolymerization of pyrrole on the surface of the gold electrode, using CV with the potential range between −0.2 and 0.8 V. Prior to electropolymerization, the surface of the gold electrode was polished with 1.0, 0.3, and 0.05 μm alumina powder and then thoroughly cleaned before use. Thereafter, the electrode was modified with N-MWCNT/GONRs and dried in air. Following that, thirty cycles of CV at 100 $mV{\cdot}s^{-1}$ in an acetate buffer solution (pH = 4.7, 25 °C) containing 25 $\mu g{\cdot}mL^{-1}$ estriol and 0.08 $mg{\cdot}mL^{-1}$ pyrrole were performed. After electropolymerization, the MIP electrode was washed using 0.3 $mol{\cdot}L^{-1}$ H_2SO_4 for 2 h to remove the imprinting molecules. In strongly acidic conditions, estriol molecules can escape from the stereo-cavity of the molecular imprinting membranes due to the destruction of

the hydrogen bonds between estriol and the molecular imprinting membranes. As a result, an electrode with an imprinted membrane that has stereo cavities for estriol detection was obtained. The above processes could be illustrated in Fig. 1.

Electroanalytical measurements

Cyclic voltammetry (CV) was used to characterize the process of MIP-modified film. It is carried out in the supporting electrolyte of 5 mmol·L^{-1} $K_3[Fe(CN)_6]$ as a redox probe at room temperature (25 °C). CV was performed from −0.2 to 0.8 V at a scan rate of 100 mV·s^{-1}.

A square wave voltammetry (SWV) detection was performed by stripping from −0.75 to 0.7 V with a potential step of 5 mV, a frequency of 25 Hz, and an amplitude of 25 mV. It was used to detect the concentration of E3. The recognition between the imprinted sensor and target molecule was observed by measuring the variation current response. The peak current of the MIP-based sensor with specific sites was large. After the MP was injected into the solution, an obvious decrease of peak current was recorded. This was assumed to be due to the MP in the solution filling the holes of the MIP on the surface of electrode, blocking the transfer. Based on the change of current signal before and after the reaction, the concentration of the MP was determined.

Electrochemical impedance spectroscopy (EIS) was obtained over the frequency range from 100 mHz to 100 kHz.

Results and discussion

Characterization of N-MWCNTs/GONRs

Figure 2 shows transmission electron microscopy (TEM) images of N-MWCNT and N-MWCNT/GONRs. Graphene sheet structures were found on both sides of the nanotubes in Fig. 2B, and the central cores of nanotubes remained slightly dark and tubelike. This type of core-shell heterostructure is termed as N-MWCNT/GONRs.

Raman spectroscopy was used to further analyze the structure of N-MWCNT and N-MWCNT/GONRs. It is obvious that D band (1300 cm^{-1}) and G band (1580 cm^{-1}) were identified for N-MWCNTs and N-MWCNT/GONRs from Fig. 2C, which was in accordance with the report by Martín and Escarpa [40]. The average size of the sp^2 carbon domain is proportional to the intensity ratio of the D and G lines (ID/IG ratio). Comparing with N-MWCNTs, N-MWCNT/GONRs showed higher ID/IG ratio which indicated N-MWCNT/GONRs suffered a decrease in the size of the sp^2-hybridized carbon domain by the unzipping procedure [41].

Samples were also characterized by Fourier transform infrared spectroscopy (Fig. 2C(a)). Band at 1390 cm^{-1} is attributed to both the C–N bond and the IR active G and D bands of graphite. The peaks around 1590 and 1620 cm^{-1} correspond to the IR active phonon mode of the N-MWCNTs [42] and the C=N stretching mode.

XPS is a useful tool to identify the elements' states in bulk material. By analysis of binding energy values, we can confirm the nature of the binding between carbon and nitrogen of N-

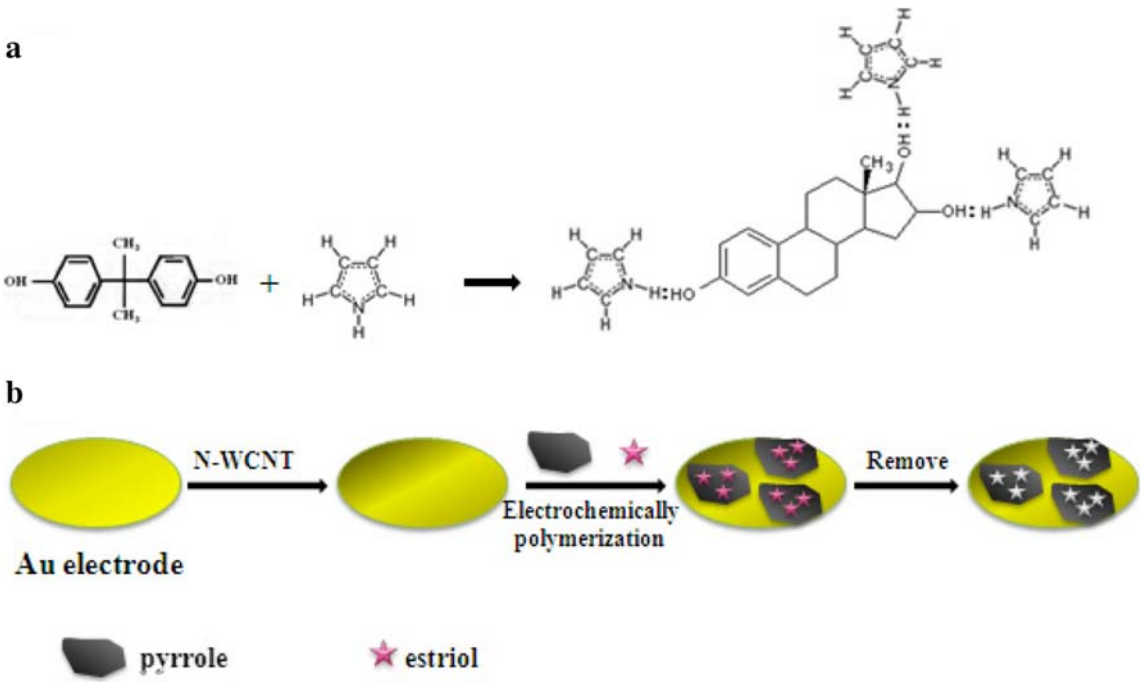

Fig. 1 **a** Schematic illustrations for electropolymerization of estriol and pyrrole, **b** the preparation of imprinted polymer-modified electrode

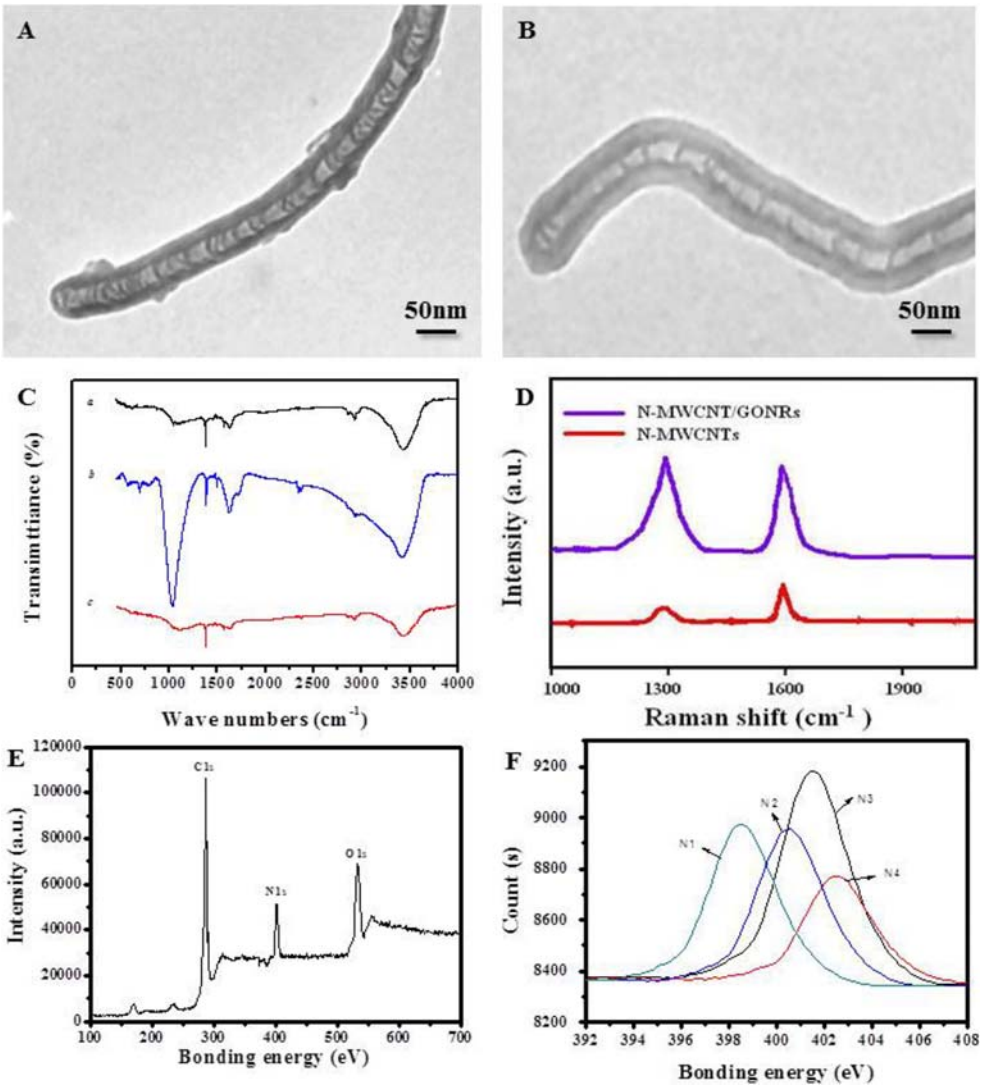

Fig. 2 Characterization of N-MWCNT/GONRs. **A** TEM of N-MWCNT, **B** TEM of N-MWCNT/GONRs, **C** FTIR spectrum of N-MWCNT/GONRs, **D** Raman spectra of N-MWCNTs and N-MWCNT/GONRs, **E** survey scan XPS of N-MWCNT/GONRs, **F** N1s XPS of N-MWCNT/GONRs

MWCNT/GONRs. As can be seen in Fig. 2E, the survey scan spectrum from XPS analysis showed the presence of the principal C1s, O1s, and N1s core levels. Figure 2F reveals the N1s XPS of N-MWCNT/GONRs. The peaks at bonding energies of 398.2 (N1), 400.2 (N2), and 401.2 eV (N3) are attributed to the pyridinic-, pyrrolic-, and quaternary-type nitrogen functionalities in the carbon lattice, respectively, and the peak at 402.2 eV (N4) corresponds to the oxidized nitrogen, which indicates that the nitrogen atoms have been doped into the N-MWCNTs successfully.

Cyclic voltammetry study of MIP-pyrrole electropolymerization

Electropolymerization of pyrrole was carried out by CV scanning in a 0.1-mol·L^{-1} acetate buffer solution (pH = 4.7, 25 °C). Results were shown in Fig. S1. The currents decreased with increasing numbers of cycles. Oxidation of pyrrole was recorded as a distinct and irreversible peak at a peak potential of 0.68 V. When the number of cycles was increased to 30, the current density of the oxidation peak became smaller, which indicated the formation of a film on the electrode surface. No reduction peak was observed during the polymerization. These results demonstrated the growth of an insulating MIP film on the Au electrode (Table 1).

Molecular recognition by MIP-modified film

According to the BET analysis, the Barret–Joyner–Halenda (BJH) desorption cumulative volume of the electropolymerization film before removing the imprinting molecules is 0.3425 cm^3/g, and the BET surface area is 117.247 m^2/g. After removal of the imprinting molecules, the BJH desorption cumulative volume increased to 0.4007 cm^3/g, and the BET surface area increased to 126.854 m^2/g. It is indicated that the imprinting molecules have been effectively removed from the electropolymerization

Table 1 Comparison of the detection limit between references and this sensor

References	Sensor structure	Linear range	Detection limit
43	Poly (glycine)-modified carbon paste electrode	2.6~100 nmol/L	0.87 nmmol/L
44	rGO-AgNPs electrode	0.1~3.0 μmol/L	21 nmmol/L
45	GC/rGO-SbNPs electrode	0.20~1.4 μmol/L	0.5 nmol/L
46	carbon paste electrode modified with ferrimagnetic nanoparticles	0.86~32.0 mg/L	0.79 mg/L
47	boron-doped diamond electrode	0.2~20 μmol/L	0.17 mol/L
48	GC electrode modified with Pt nano-clusters/multi-walled carbon nanotubes	1.0~75 μmol/L	620 nmol/L

film. Integrated BET and SEM, imprinting molecules have been effectively removed from the electropolymerization film.

Samples were also characterized by Fourier transform infrared spectroscopy (Fig. 2C). Band at 1390 cm^{-1} is attributed to both the C–N bond and the IR-active G and D bands of graphite. The peak around 1590 and 1620 cm^{-1} correspond to the IR-active phonon mode of the N-MWCNTs [42] and the C=N stretching mode (Fig. 2C(a)). After the electropolymerization of MIP film at N-MWCNT/GONRs modified Au electrode, the peak around 1000cm-1 correspond to the C-O stretching vibration band, the peak around 1490 cm-1 is attributed to the splitting of the methylene scissoring mode, the peaks around 3300cm-1 and 690cm-1 correspond to the O-H stretching vibration and bending vibration (Fig. 1C (b)). It is indicated that MIP film (pyrrole and E3) has been formed on the electrode. After the MIPs/N-MWCNT/GONRs/Au electrode was immersed in 0.3 mol·L^{-1} H_2SO_4 for 2 h, the peak around 1000 cm^{-1} disappeared, which suggested that the template molecules has been removed from the MIP film (Fig. 2C(c)).

CV results of the MIP films were recorded in 5 mmol·L^{-1} $K_3[Fe(CN)_6]$ solution, as shown in Fig. 3. During this procedure, $K_3[Fe(CN)_6]$ was used as the mediator between imprinted electrodes and substrate solutions. Figure 3a was a CV curve of $K_3[Fe(CN)_6]$ at the bare Au electrode, showing a pair of redox peaks. Figure 3b and c showed the CV for $[Fe(CN)_6]^{3+}$ obtained at N-MWCNT/GONR-modified electrode and N-MWCNT-modified electrode, respectively. It was obvious that the current response at N-MWCNT/GONR-modified electrode became larger than that of bare Au electrode and N-MWCNT-modified electrode. Electroactive surface area was calculated. According to the formula below (Eq.1) [49]. The electroactive surface areas of bare Au electrode, Au electrode modified with N-MWCNT/GONR, and Au electrode modified with N-MWCNT were 0.047, 0.059, and 0.051 cm^2.

$$I_p = 268,600 n^{3/2} A D^{1/2} C v^{1/2} \quad (1)$$

n: the electron charge transfer number, $n = 1$;

D: the diffusion coefficient (6×10^{-6} for $[Fe(CN)_6]^{4-}$), cm^2/s;

C: the concentration of the reaction species in the electrolyte (5×10^{-6} for $[Fe(CN)_6]^{4-}$ here), mol/cm^3;

v: the scan rate, V/s;

A: the electroactive surface area, cm^2;

I_p: the peak current, A.

For the MIP Au electrode, there was no peak as shown in Fig. 3d. This was likely because electron transfer was blocked by the non-conducting estriol membranes covering the electrode. After removal of estriol, a visible oxidation-reduction peak was obtained (curve e). This could be explained that after the removal of estriol, the formation of vacant recognition sites or binding cavities made electronic transfer possible. Then $K_3[Fe(CN)_6]$ could pass through the cavity and reach the surface of the electrode more easily. The decrease of peak

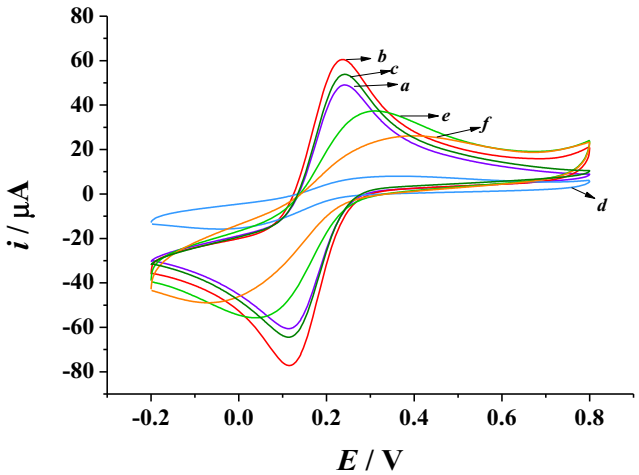

Fig. 3 Cyclic voltammograms of $K_3[Fe(CN)_6]$ (**a**) bare Au electrode, (**b**) Au electrode modified with N-MWCNT/GONR, (**c**) Au electrode modified with N-MWCNT, (**d**) MIP-modified Au electrode before removal of the imprinted estriol molecules, (**e**) MIP-modified Au electrode after removal of the imprinted estriol molecules, (**f**) MI-modified Au electrode after interaction with estriol

current from curve e to curve f could be attributed to the obstruction of the access of $K_3[Fe(CN)_6]$ through the MIP film after estriol rebinding. Thus, the interaction between the estriol and the MIP film determines the electron transfer of the $[Fe(CN)_6]^{3-}/[Fe(CN)_6]^{4-}$ ion pair on the electrode surface.

Optimization of experimental conditions

As shown in Fig. 4a, with the increasing of the N-MWCNT/GONR concentration from 0.5 to 4.0 mg·mL^{-1}, the current response increased gradually, and reached the maximum at 2.0 mg·mL^{-1}. However, with further increasing of the concentration of N-MWCNT/GONRs, there is no obvious change. It could be attributed to the increase of film thickness, leading to an increase of interface electron transfer resistance, making the electron transfer more difficultly. Based on the results, 2.0 mg·mL^{-1} was selected for following experiments.

The effect of pH on the current decrease was examined in the range from pH 4.0 to 5.8, as shown in Fig. 3b. The electrochemical reaction of MIP involves proton transfer and electron transfer. The peak current increased with the pH from 4.0 to 4.7, and then it decreased with further increase, which might be due to the proton transfer and electron transfer reaching the equilibrium at pH 4.7. Therefore, further experiments were carried out at pH 4.7.

It is well known that the sensitivity of the imprinted sensor is dictated by the amount of effective imprinted sites on the sensor surface. The ratio of template to monomer was found to play a key role in the performance of sensor because the template–monomer ratio of MIP determines the number of binding sites available for selective rebinding of estriol. Therefore, the ratio of estriol and pyrrole was studied by varying the concentration of pyrrole and keeping that of estriol at 10 mg·L^{-1}, as shown in Fig. 4c. It was obvious that the largest current response was obtained when template–monomer ratio was 1:4. When the ratio was less than 1:4, the current response was small due to the limited binding sites available. When the ratio was higher than 1:4, the current response kept stable. Pyrrole of 80 mg·L^{-1} was determined in the experiment. In the experiment, H_2SO_4 was chosen as the eluent.

The effect of H_2SO_4 concentration was performed, and the result was shown in Fig. 4d. The current increased with the elution concentration range from 0.1 mol·L^{-1} to 0.3 mol·L^{-1} and decreased with the elution concentration range from 0.3 mol·L^{-1} to 0.5 mol·L^{-1}. Therefore, 0.3 mol·L^{-1} H_2SO_4 was selected in the following experiment.

Figure 4e showed the effect of elution time. The current increased with the elution time up to the 2 h and remained constant subsequently. Thus, 2 h elution time was finalized in the subsequent test.

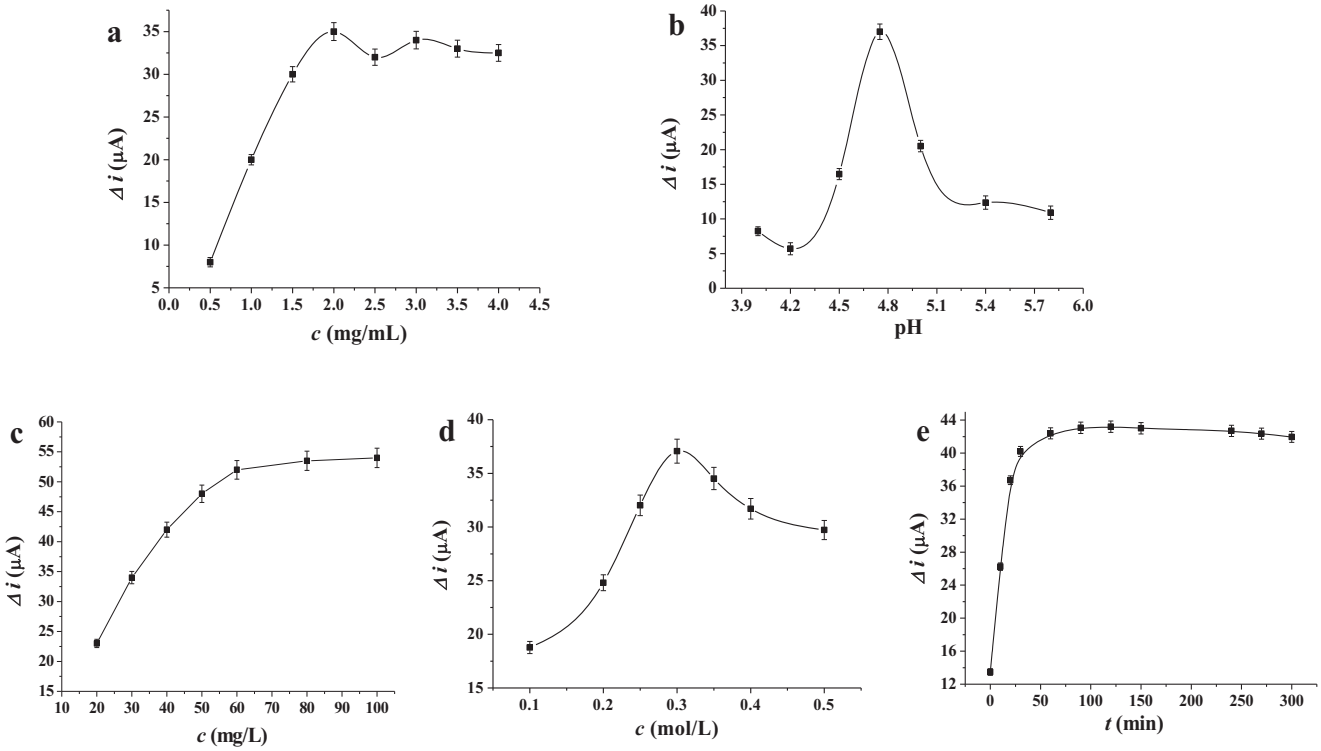

Fig. 4 Effect of (**a**) N-MWCNT/GONR concentration, (**b**) pH, (**c**) concentration of pyrrole, (**d**) concentration of H_2SO_4, and (**e**) elution time on respond signals (SWV detection was performed by stripping from −0.75 to 0.7 V with a potential step of 5 mV, a frequency of 25 Hz, and an amplitude of 25 mV after and before removal of the imprinted estriol molecules)

Impedance measurement

The electrochemical impedance technique is employed to evaluate the interface properties of surface-modified sensors by detecting impedance change during electrode modification process. The fabrication process was characterized by using electrochemical impedance spectroscopy (EIS). In the Nyquist diagram, the semicircle diameter of electrochemical impedance spectroscopy (EIS) is equal to R_{et}.

Figure 5 showed the Nyquist diagrams of electrochemical impedance spectra at the different fabricated electrode recorded in 5 mmol·L^{-1} $K_3[Fe(CN)_6]$ solution. Almost a straight line could be observed for bare Au electrode (curve a), which implied a very fast electron transfer process with a diffusional limiting step of the electrochemical process. After being coated with N-MWCNT/GONRs, the EIS of the modified electrode (curve b) was similar to that of the bare electrode. It may be that the N-MWCNT/GONRs are immobilized on the electrode similar to a conducting wire, which makes it easier for the electron transfer. After the electropolymerization of MIP film at N-MWCNT/GONR-modified Au electrode (curve d), the impedance was significantly enlarged and the semicircle diameter was about 4200 Ω. This result indicated that MIP film has been formed and it has obstruction effect, which resulted in reducing electron transfer rate or increasing resistance to the flow of electrons. The decrease of resistance (curve c) was observed after the MIPs/N-MWCNT/GONRs/Au electrode was immersed in 0.3 mol·L^{-1} H_2SO_4 for 2 h. It was indicated that template molecules had been removed from the MIP film. And then immersing the MIPs/N-MWCNT/GONRs/Au electrode in estriol solution, the resistance increased again (curve e), which could be attributed to the rebinding of estriol into the imprinted cavities and the blocking of the arrival of the probe onto the electrode surface. This verified that the MIP film has good capability to distinguish the target molecules.

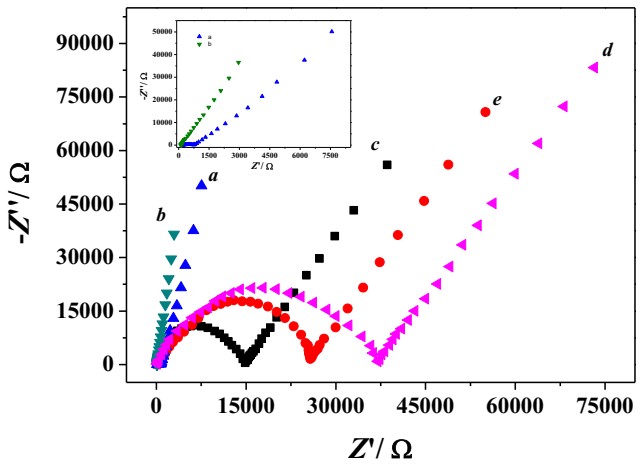

Fig. 5 Electrochemical impedance spectra recorded in $K_3[Fe(CN)_6]$ solution at (**a**) bare Au electrode, (**b**) Au electrode modified with N-MWCNT/GONRs, (**c**) MIP-modified Au electrode after removal of the imprinted estriol molecules, (**d**) MIP-modified Au electrode before removal of the imprinted estriol molecules, (**e**) MIP-modified Au electrode after interaction with estriol

Calibration curve and sensitivity

Under the optimum conditions, the calibration curve to different concentrations of estriol was studied. The amperometric responses of the modified Au electrode to estriol are depicted in Fig. 6. After adding analyte solutions with different concentrations, the oxidation currents of specific analytes were monitored. It exhibited good linear relationships between the current change and the concentration of estriol in the range from 0.1 to 20 μg·mL^{-1} with the detection limit of 2 ng·mL^{-1}, which was better than some other results by researchers [43–48].

Reproducibility selectivity and stability

To evaluate the reproducibility of the sensors, a series of five electrodes were prepared for the detection of estriol. The relative standard deviation (RSD) of the measurements for the five electrodes was 4.7%.

The oxidation peak currents of 10 μg·mL^{-1} estriol in the absence and presence of interferents were measured by the sensor. It was found that the deviations of 50-fold concentrations of estradiol, diethylstilbestrol, oestrone, bisphenol A, and ethinyloestradiol were 18.3, 4.5, 6.7, 6.2, and 8.4%. Except estradiol, others had minor influence on the signals of estriol. Because of similar structure, the deviation is higher than others but also acceptable. Uric acid, ascorbic acid, and some ions such as 100-fold concentrations of K^+, Na^+, Ca^{2+}, Mg^{2+}, Al^{3+}, Zn^{2+}, and Cu^{2+} had no influence on estriol determination.

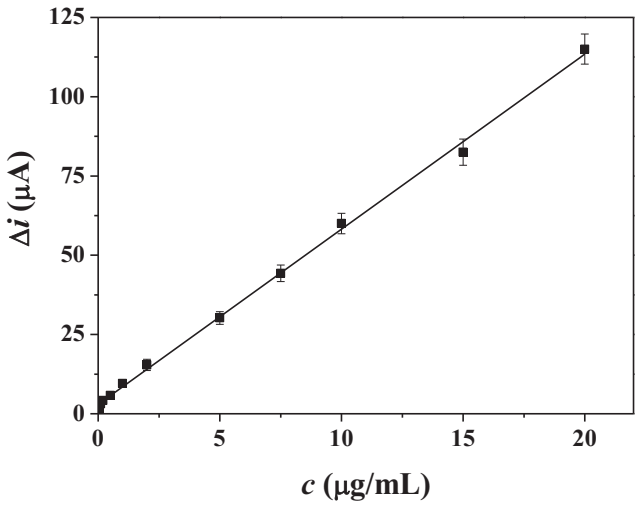

Fig. 6 Calibration curve for detection with at different concentrations of estriol

To test the stability of the sensor, it was dipped in water at 4 °C after each use. After 4 days, the current only decreased to about 93% of its initial value. After 30 days, the current only decreased to about 80.2% of its initial value. Therefore, the proposed sensor possessed acceptable storage stability.

Application

To evaluate the applicability of the proposed sensor, the concentration of estriol in human serum samples and water samples were determined applying the standard addition method. The recovery was in the range of 93.7~105.4% and 94.2~106.2% respectively, indicating that the imprinted sensor might be preliminarily applied for the determination of estriol in clinical samples and in real water samples.

To further investigate the availability of this sensor for estriol detection, a comparison of the results obtained by the proposed sensor and LC–MS method were made. Estriol content determined by the two methods agreed well, and the plot of estriol contents obtained by the two methods gave a straight line with a correlation coefficient of 0.996 (Fig. S2), indicating the proposed sensor might be used for the detection of estriol.

Conclusions

A novel sensitive molecularly imprinted electrochemical sensor based on a core-shell N-MWCNT/GONR-modified Au electrode has been developed for estriol determination. The cavity formed exhibits high specificity, excellent selectivity, and stability in the target solution. The recognition between the imprinted sensor and target molecules was observed by measuring the variation amperometric response of the oxidation–reduction probe on electrode. It provides a promising tool for estriol detection in clinical samples and in real water samples.

Acknowledgements This study was supported by National Major Projects on Water Pollution Control and Management Technology (no. 2017ZX07501003, no. 2017ZX07502003-06), the Natural Science Foundation of Shandong Province (ZR2019QEE022), and the Special Project of Taishan Scholar Construction Engineering (ts201712084).

References

1. Lonning PE, Skulstad PJ (1989) Alterations in the urine excretion of estrogen metabolites in breast cancer women treated with aminoglutethimide. Steroid Biochem 33:565–571
2. Kolpin DW, Furlong ET, Meyer MT, Thurman EM, Zaugg SD, Barber LB, Buxton HT (2002) Pharmaceuticals, hormones, and other organic wastewater contaminants in U.S. streams, 1999-2000: A national reconnaissance. Environ Sci Technol 36:1202–1211
3. Huang X, Yuan D, Huang B (2008) Determination of steroid sex hormones in urine matrix by stir bar sorptive extraction based on monolithic material and liquid chromatography with diode array detection. Talanta 75:172–177
4. Ingrand V, Herry G, Beausse J, de Roubin MR (2003) Analysis of steroid hormones in effluents of wastewater treatment plants by liquid chromatoraphy–tandem mass spectrometry. J Chromatogr A 1020:99–104
5. Penalver A, Pocurull E, Borrull F et al (2002) Method based on solid-phase microextraction–high-performance liquid chromatography with UV and electrochemical detection to determine estrogenic compounds in water samples. J Chromatogr A 964:153–160
6. Koh YKK, Chiu TY, Boobis A, Cartmell E, Lester JN, Scrimshaw MD (2007) Determination of steroid estrogens in wastewater by high performance liquid chromatography–tandem mass spectrometry. J Chromatogr A 1173:81–87
7. Fuh MR, Huang SY, Lin TY (2004) Determination of residual anabolic steroid in meat by gas chromatography–ion trap–mass spectrometer. Talanta 64:408–414
8. Santos KD, Braga OC, Vieira IC, Spinelli A (2010) Electroanalytical determination of estriol hormone using a boron-doped diamond electrode. Talanta 80:1999–2000
9. Caruane AD, Martin KLS, Rafael PS, Ivana C (2018) Reduced graphene oxide modified with silver nanoparticles for the electrochemical detection of estriol. J Electroanal Chem 809:67–73
10. Ivana C, Fernando HC, Sergio ASM (2015) A synergistic combination of reduced graphene oxide and antimony nanoparticles for estriol hormone detection. Sensor Actuat B 210:453–459
11. Portaccio M, Tuoro DD, Arduini F et al (2010) A thionine-modified carbon paste amperometric biosensor for catechol and bisphenol A determination. Biosens Bioelectron 25:2003–2008
12. Du Y, Gao X, Ye X et al (2014) Composition and architecture-engineered Au–SnO2/GNs-SWCNTs nanocomposites as ultrasensitive and robust electrochemical sensor for antioxidant additives in foods. Sens Actuat B 203:926–934
13. Yin HS, Cui L, Ai SY et al (2010) Electrochemical determination of bisphenol A at Mg–Al–CO_3 layered double hydroxide modified glassy carbon electrode. Electrochim Acta 55:603–610
14. Engin E, Hüseyin Ç, Nevin E et al (2015) A new generation electrochemical sensor based on graphene nanosheets/gold nanoparticles/nafion nanocomposite for determination of Silodosin. Electrochim Acta 157:252–257
15. Zhang Z, Cai R, Long F, Wang J (2015) Development and application of tetrabromobisphenol A imprinted electrochemical sensor based on graphene/carbon nanotubes three-dimensional nanocomposites modified carbon electrode. Talanta 134:435–442
16. Wang L, Wang Y, Zhuang Q (2019) Simple self-referenced ratiometric electrochemical sensor for dopamine detection using electrochemically pretreated glassy carbon electrode modified by acid-treated multiwalled carbon nanotube. J Electroanal Chem 851: 113446
17. Abbas A, Hosein K, Hasan B et al (2014) Facile simultaneous electrochemical determination of codeine and acetaminophen in pharmaceutical samples and biological fluids by graphene–$CoFe_2O_4$ nanocomposite modified carbon paste electrode. Sens Actuator B 203:909–918
18. Pumera M (2010) Graphene-based nanomaterials and their electrochemistry. Chem Soc Rev 39:4146–4157
19. Zhao M, Ma X, Xiao H (2019) Regulation of the degree of hydrogenation and electrochemical properties of graphene generated by electrochemical cathodic exfoliation by using different solvents. Electrochem Commun 103:77–82
20. Sun CL, Chang CT, Lee HH, Zhou J, Wang J, Sham TK, Pong WF (2011) Microwave-assisted synthesis of a core-shell MWCNT/

GONR heterostructure for the electrochemical detection of ascorbic acid, dopamine, and uric acid. ACS Nano 5:7788–7795
21. Lee KR, Lee KU, Lee JW et al (2010) Electrochemical oxygen reduction on nitrogen doped graphene sheets in acid media. Electrochem Commun 12:1052–1055
22. Li XL, Wang HL, Robinson JT, Sanchez H, Diankov G, Dai H (2009) Simultaneous nitrogen doping and reduction of graphene oxide. J Am Chem Soc 131:15939–15944
23. Long DH, Li W, Ling LC, Miyawaki J, Mochida I, Yoon SH (2010) Preparation of nitrogen-doped graphene sheets by a combined chemical and hydrothermal reduction of graphene oxide. Langmuir 26:16096–16102
24. Qu LT, Liu Y, Baek JB, Dai L (2010) Nitrogen-doped graphene as efficient metal-free electrocatalyst for oxygen reduction in fuel cells. ACS Nano 4:1321–1326
25. Reddy ALM, Srivastava A, Gowda SR et al (2010) Synthesis of nitrogen-doped graphene films for lithium battery application. ACS Nano 4:6337–6342
26. Alexeyeva N, Shulga E, Kisand V et al (2010) Synthesis of nitrogen-doped graphene films for lithium battery application. J Electroanal Chem 648:169–175
27. Li H, Kang W, Wang L et al (2013) Synthesis of three-dimensional flowerlike nitrogen-doped carbons by a copyrolysis route and the effect of nitrogen species on the electrocatalytic activity in oxygen reduction reaction. Carbon 54:249–257
28. Vikkisk M, Kruusenberg I, Joost U et al (2013) Electrocatalysis of oxygen reduction on nitrogen-containing multi-walled carbon nanotube modified glassy carbon electrodes. Electrochim Acta 87: 709–716
29. Arand M, Fallahi P (2013) Voltammetric determination of rivastigmine in pharmaceutical and biological samples using molecularly imprinted polymer modified carbon paste electrode. Sens Actuator B 188:797–805
30. Ma J, Yuan LH, Ding MJ, Wang S, Ren F, Zhang J, du S, Li F, Zhou X (2011) The study of core–shell molecularly imprinted polymers of 17β-estradiol on the surface of silica nanoparticles. Biosens Bioelectron 26:2791–2795
31. Zhou Y, James DK, Tour JM (2012) New routes to graphene, graphene oxide and their related applications. Adv Mater 24: 4924–4955
32. Wang S, Wang RY, Wu XL et al (2012) Magnetic molecularly imprinted nanoparticles based on dendritic-grafting modification for determination of estrogens in plasma samples. J Chromatogra B 905:105–112
33. Xie CG, Li HF, Li SQ, Wu J, Zhang Z (2010) Surface molecular self-assembly for organophosphate pesticide imprinting in electropolymerized poly(p-aminothiophenol) membranes on a gold nanoparticle modified glassy carbon electrode. Anal Chem 82:241–249
34. Deng M, Yang X, Silke M et al (2011) Electrochemical deposition of polypyrrole/graphene oxide composite on microelectrodes towards tuning the electrochemical properties of neural probes. Sens Actuator B 158:176–184
35. Xing X, Liu S, Yu J, Lian W, Huang J (2012) Electrochemical sensor based on molecularly imprinted film at polypyrrole-sulfonated graphene/hyaluronic acid-multiwalled carbon nanotubes modified electrode for determination of tryptamine. Biosens Bioelectron 31:277–283
36. Zhu C, Zhai J, Wen D et al (2012) Graphene oxide/polypyrrole nanocomposites: one-step electrochemical doping, coating and synergistic effect for energy storage. J Mater Chem 22:6300–6306
37. Yang Y, Fang G, Wang X, Pan M, Qian H, Liu H, Wang S (2014) Sensitive and selective electrochemical determination of quinoxaline-2-carboxylic acid based on bilayer of novel poly(pyrrole) functional composite using one-step electro-polymerization and molecularly imprinted poly(o-phenylenediamine). Anal Chim Acta 806:136–143
38. Yu DS, Zhang Q, Dai LM (2010) Highly efficient metal-free growth of nitrogen-doped single-walled carbon nanotubes on plasma-etched substrates for oxygen reduction. J Am Chem Soc 132: 15127–15129
39. Zhang L, Xia Z (2011) Mechanisms of oxygen reduction reaction on nitrogen-doped graphene for fuel cells. J Phys Chem C 115: 11170–11176
40. Martín A, Escarpa A (2014) Graphene: the cutting–edge interaction between chemistry and electrochemistry. TrAC Trend Anal Chem 56:13–26
41. Cheng M, Yang R, Zhang L et al (2012) Restoration of graphene from graphene oxide by defect repair. Carbon 50:2581–2587
42. Wu TM, Lin YW, Liao CS (2005) Preparation and characterization of polyaniline/multi-walled carbon nanotube composites. Carbon 43:734–740
43. Manjunatha JG (2017) Electroanalysis of estriol hormone using electrochemical sensor. Sens BioSens Res 16:79–84
44. Caruane AD, Martin KLS, Rafael PS et al (2018) Reduced graphene oxide modified with silver nanoparticles for the electrochemical detection of estriol. J Electro Chem 809:67–73
45. Cesarino I, Cincotto FH, Machado SAS (2015) A synergistic combination of reduced graphene oxide and antimony nanoparticles for estriol hormone detection. Sensors Actuators B Chem 210:453–459
46. Silveira JP, Piovesan JV, Spinelli A (2017) Carbon paste electrode modified with ferrimagnetic nanoparticles for voltammetric detection of the hormone estriol. Microchem J 133:22–30
47. Santos KD, Braga OC, Vieira IC, Spinelli A (2010) Electroanalytical determination of estriol hormone using a boron-doped diamond electrode. Talanta 80:1999–2006
48. Lin X, Li Y (2006) A sensitive determination of estrogens with a Pt nano-clusters/multiwalled carbon nanotubes modified glassy carbon electrode. Biosens Bioelectron 22:253
49. Zhu P, Zhao Y (2019) Cyclic voltammetry measurements of electroactive surface area of porous nickel: peak current and peak charge methods and diffusion layer effect. Mater. Chem. And Phys 233:60–67